

CliQ-RRG: Clinical-Knowledge Guided Disease-aware Visual–Textual Alignment for QA-Style Radiology Report Generation

Anonymous ACL submission

Abstract

Radiology reports are essential for diagnostic reasoning and patient care, yet their manual preparation is time-consuming and cognitively demanding. Automatic radiology report generation (RRG) offers a scalable alternative, but existing models often produce lengthy, unstructured narratives that overlook diagnostic cues and multi-view information. We present Clinical-Knowledge Guided Disease-aware Visual–Textual Alignment for QA-Style Radiology Report Generation (CliQ-RRG), a unified two-stage framework for interpretable and clinically grounded reporting. In Stage 1, CliQ-RRG employs a Disease-aware Visual–Textual Alignment module that aligns image and text representations using predicted disease embeddings, reinforced by a Prior-Guided Attention Module (PrAM) to capture multi-view dependencies across current and prior scans. In Stage 2, domain-specific clinical knowledge is injected into intermediate textual representations, and a large language model restructures them into concise, interpretable question–answer (QA) pairs with diagnostic summaries. Experiments on two public chest X-ray benchmarks demonstrate that CliQ-RRG consistently outperforms prior methods across both lexical and clinical metrics, generating accurate and clinically coherent QA-style radiology reports. Code is available at <https://anonymous.4open.science/r/CliQ-RRG>.

1 Introduction

Radiology report generation (RRG) is vital for chest X-ray (CXR) interpretation, requiring substantial clinical expertise and reasoning (Jin et al., 2024). Manual interpretation, however, remains time-consuming and cognitively demanding, even for experts (Liu et al., 2025a; Park et al., 2025). As imaging volumes rise, radiologists face increasing workload, often affecting report quality and diagnostic accuracy. Consequently, automated RRG has emerged as a promising solution (Hou et al.,

2023; Liang et al., 2024; Luo et al., 2024), yet most methods emphasize disease-specific regions, overlooking broader contextual information.

Recent studies have proposed advanced techniques to improve automatic RRG. Li et al. (2024b) integrates graph-enhanced and regional features to describe normal and abnormal findings, yet outputs remain lengthy and less interpretable. To embed clinical knowledge, Hou et al. (2025) and Sun et al. (2025) retrieve domain-specific information, but the generated texts lack diagnostic coherence. Huang et al. (2025) aligns visual and textual features via a cross-modal adapter; however, the approach is inefficient and overlooks supervised labels that strengthen the alignment. Dual-view RRG methods (Chen et al., 2021; Yang et al., 2023) differentiate radiographic views but miss fine anatomical and contextual relations across scans, limiting multi-view consistency in generated reports.

Despite progress in RRG (Zhang et al., 2020; Yan and Pei, 2022), existing methods face four key limitations (Fig. 1). **(G1) Prior works** (Jin et al., 2024; Luo et al., 2024; Wang et al., 2025) mainly

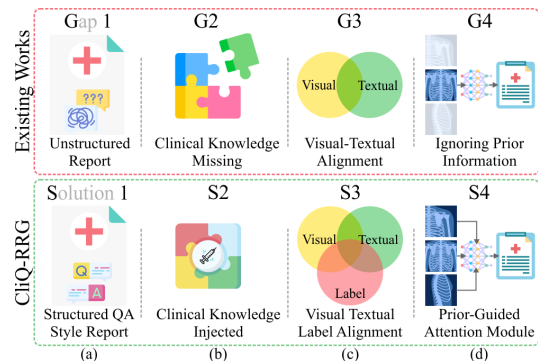


Figure 1: Comparison with existing methods. Existing approaches generate unstructured reports, neglect prior scans, and lacks in clinical knowledge, whereas CliQ-RRG produces QA-style reports, injects clinical knowledge, performs visual–textual–label alignment, and leverages prior scans via prior-guided attention.

generate long free-text narratives, in which key findings are embedded within paragraphs rather than presented in a structured form. Existing studies have noted limitations of lengthy and inconsistently structured clinical text (Kell et al., 2024; Pattnayak et al., 2025; Schwartz et al., 2011). We therefore explore a QA-style reformulation to make findings explicit and easier to retrieve, aiming to improve structural clarity rather than replace narrative reports. **(G2)** Many studies (Yan et al., 2023; Bu et al., 2024a; Gu et al., 2024) rely solely on image-report pairs, which may yield fluent but underspecified descriptions, especially for subtle findings. We incorporate external clinical knowledge at the intermediate stage to promote more specific, clinically grounded expressions and strengthen alignment between visual evidence and generated text. **(G3)** Recent studies (Li et al., 2023; Shen et al., 2024; Xiao et al., 2025) align visual and textual modalities but often neglect diagnostic labels as supervisory signals for joint embedding learning, unlike prompt-based approaches (Jin et al., 2024). We integrate predicted diagnostic labels directly into a tri-channel contrastive alignment objective, structuring the joint visual–textual space based on diagnostic similarity. **(G4)** While several methods (Hou et al., 2023; Gu et al., 2025; Liu et al., 2025b) leverage historical information, most standard approaches do not explicitly fuse prior scans at the visual representation level. We introduce prior-image fusion before alignment to capture temporal context within the learned feature space.

We present Clinical-Knowledge Guided Disease-aware Visual–Textual Alignment for QA-Style Radiology Report Generation (CliQ-RRG), a unified framework that integrates domain knowledge, leverages multi-view priors, and performs disease-aware alignment. As shown in Fig. 1, CliQ-RRG addresses limitations of prior RRG methods. **(S1)** It reformulates free-text reports into clinically interpretable QA-style outputs. **(S2)** It injects external clinical knowledge to enable reasoning beyond data-driven correlations. **(S3)** It aligns visual and textual representations via predicted disease embeddings to achieve semantically grounded features. **(S4)** It incorporates multi-view information from prior examinations through a prior-guided attention mechanism to enhance contextual understanding. Extensive experiments on **MIMIC-CXR** and **IU X-Ray** show that CliQ-RRG consistently outperforms state-of-the-art methods in radiology report generation. Our main contributions are threefold:

- To the best of our knowledge, CliQ-RRG is the first framework to leverage contrastive alignment for QA-style radiology report generation, restructuring unstructured narratives into concise, structured question-answer pairs.

- We introduce a Disease-aware Visual-Textual Alignment module that aligns image and text representations via predicted disease embeddings, guided by a Prior-Guided Attention Module for multi-view contextual integration.

- We design a knowledge-guided generation pipeline that enriches intermediate reports with retrieved clinical knowledge and uses a large language model to restructure the final QA-style report.

2 Proposed Approach

2.1 Problem Formulation and Overview

Let $\mathcal{T} = \{(I_k, R_k, L_k)\}_{k=1}^n$ be the training set of n studies, each with a CXR $I_k \in \mathbb{R}^{h \times w \times (v+1)}$, associated report R_k , and predicted disease labels L_k , where v is the number of prior scans ($v = 0$ if unavailable), and h, w are image dimensions. Our objective is to generate a QA-style report $R_{qa}(q_i, a_i)$, where each question q_i targets a clinical finding, and the answer $a_i \in \{\text{Yes}, \text{No}\}$ is grounded in visual evidence from I . The value m is the total number of generated question–answer pairs. We hypothesize that aligning visual and textual representations with predicted disease labels allows our framework to generate QA-style radiology reports. We formalize the generation process as:

$$R_{qa}(q_k, a_k) = \text{CliQ-RRG}(I, R, L) \quad (1)$$

Our proposed framework, CliQ-RRG, operates in two stages, illustrated in Fig. 2. STAGE 1 employs a disease-aware visual–textual alignment module to align visual features from current and prior chest X-rays with textual representations and predicted disease labels in a unified embedding space. A prior-guided attention module further captures multi-view information from prior scans, enhancing temporal and anatomical consistency. In STAGE 2, a text decoder generates an intermediate report, which we enhance by appending top- k_t clinically relevant knowledge tokens from a clinical knowledge. Finally, an LLM restructures the knowledge-injected report into a concise QA-style format with question–answer pairs and a clinical summary.

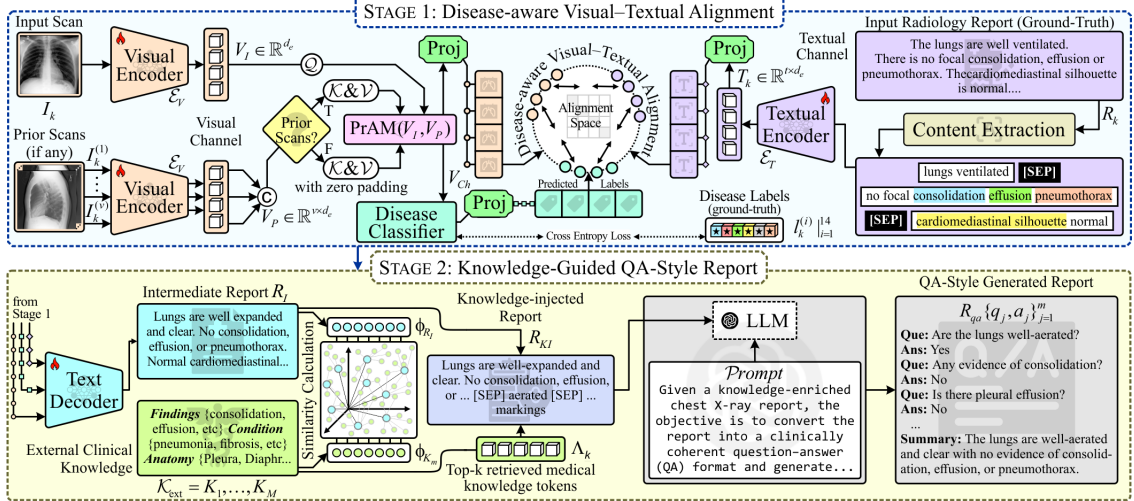


Figure 2: Overview of the proposed CliQ-RRG framework. STAGE 1: Disease-aware Visual-Textual Alignment aligns image and text features using predicted disease embeddings, while the Prior-Guided Attention Module (PrAM) integrates multi-view information from current and prior scans. STAGE 2: Knowledge-Guided QA-Style Report Generation enriches the intermediate report with retrieved clinical knowledge and employs a large language model to produce concise question–answer pairs and a diagnostic summary.

2.2 STAGE 1: Disease-aware Visual-Textual Alignment

Visual Channel: Let I_k denote the current CXR and $I_k^{(j)}$ the set of v prior scans for the k^{th} patient ($v \geq 0$). We use the BioMedCLIP (Zhang et al., 2025) visual encoder $\mathcal{E}_V(\cdot)$ to extract image features. The current view is encoded as $V_I = \mathcal{E}_V(I_k)$, and each prior view as $V_P^{(j)} = \mathcal{E}_V(I_k^{(j)})$. Prior features are concatenated to form a contextual representation $V_P = \text{Concat}(V_P^{(1)}, \dots, V_P^{(v)})$, zero-padded when $v = 0$. The visual channel representation is defined as $V_{ch} = \text{PrAM}(V_I, V_P)$, where PrAM fuses the current image features V_I and prior image features V_P , capturing both current and multi-view information.

Prior-guided Attention Module: To handle variable image counts across studies, which complicate concatenation and hinder cross-modal alignment, we introduce the Prior-Guided Attention Module (PrAM). PrAM integrates multi-view information from prior scans through a cross-attention mechanism (Vaswani et al., 2017). The current image feature $V_I \in \mathbb{R}^{d_e}$ serves as the query \mathcal{Q} , and the prior features $V_P \in \mathbb{R}^{v \times d_e}$ act as both keys \mathcal{K} and values \mathcal{V} , where d_e is the shared embedding dimension. The output is computed as:

$$\text{PrAM}(V_I, V_P) = \text{softmax}\left(\frac{V_I V_P^\top}{\sqrt{d_e}}\right) \cdot V_P \quad (2)$$

producing a unified representation that preserves multi-view context while maintaining consistent

dimensionality for contrastive alignment.

Textual Channel: To process radiology reports R_k , we construct a textual channel T_{ch} that encodes clinical information. Following (Yan et al., 2023; Liu et al., 2025a, 2024c), we extract a sequence of t_c salient clinical phrases from R_k , separated by [SEP] tokens, as shown in Fig. 2. This sequence is passed through a textual encoder $\mathcal{E}_T(\cdot)$, instantiated as CXR-BERT (Boecking et al., 2022), yielding textual features $T_k = \mathcal{E}_T(R_k) \in \mathbb{R}^{t_c \times d_e}$. These representations enable alignment with visual and label modalities during contrastive learning. During inference, ground-truth reports are unavailable; therefore, T_{ch} is not used. The decoder relies solely on the visual channel V_{ch} and predicted diagnostic labels L_{ch} . Since V_{ch} has been aligned with T_{ch} during training, it encodes the necessary semantic information to guide generation.

Disease Classifier: To capture disease-relevant supervision, we design a disease classifier that predicts diagnostic labels (L_{ch}) from the visual channel features $V_{ch} \in \mathbb{R}^{d_e}$. The classifier computes disease logits using a cross-attention mechanism (Vaswani et al., 2017) and is optimized with a cross-entropy loss:

$$L_{ch} = \text{Softmax}\left(\frac{V_{ch} \Phi^\top}{\sqrt{d_e}}\right) \quad (3)$$

$$\mathcal{L}_{CE} = \text{CrossEntropy}(L_{ch}, L_{gt}) \quad (4)$$

where $\Phi \in \mathbb{R}^{d_e \times d_e}$ is a learnable disease embedding matrix and L_{gt} represents the ground-truth disease

224 labels extracted using CheXbert (Smit et al., 2020).
 225 Each label $l_k^{(i)} \in \{-1, 0, 1, 2\}$ denotes uncertainty,
 226 negative, positive, or not mentioned, respectively.
 227 We retain the first 13 disease categories to identify
 228 reports with positive or uncertain findings.

229 **Disease-aware Visual–Textual Contrast:** Building
 230 on prior contrastive and alignment-based RRG
 231 methods that align visual and textual representations
 232 through learned knowledge bases or region-
 233 level correspondence (Yang et al., 2023; Chen et al.,
 234 2024), we propose Disease-aware Visual–Textual
 235 Contrast (Di-VTC), which adapts contrastive learning
 236 to the generative setting of QA-style radiol-
 237 ogy report generation. While prior work applies
 238 contrastive learning primarily in discriminative set-
 239 tings, Di-VTC learns the parameters θ_V and θ_T of
 240 the visual (\mathcal{E}_V) and textual (\mathcal{E}_T) encoders to align
 241 visual (V_{ch}) and textual (T_{ch}) representations in a
 242 shared embedding space. For samples g and h in
 243 a batch B , the channel features are projected and
 244 L_2 -normalized to yield $\hat{v}_g = \text{Norm}(\text{Proj}(V_{ch}^{(g)}))$ and
 245 $\hat{t}_h = \text{Norm}(\text{Proj}(T_{ch}^{(h)}))$. A pair is treated as positive
 246 if their predicted diagnostic labels are similar, de-
 247 noted as $l_g \approx l_h$, where two samples are considered
 248 similar when their disease label vectors are iden-
 249 tical or satisfy a predefined similarity threshold;
 250 otherwise, the pair is treated as negative. As shown
 251 in Fig. 3, Di-VTC employs a push–pull dynamic
 252 that maximizes $\hat{v}_g^\top \hat{t}_h$ for positive pairs and mini-
 253 mizes it for negative pairs. The model is optimized
 254 using a bidirectional contrastive loss $\mathcal{L}_{\text{Di-VTC}}$ over
 255 θ_V and θ_T .

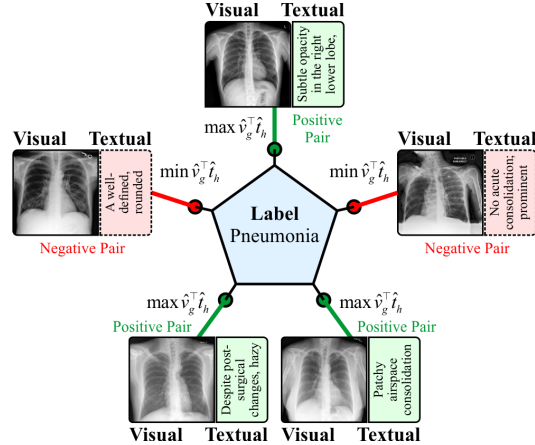
$$\min_{\{\theta_V, \theta_T\}} \mathcal{L}_{\text{Di-VTC}} = \mathcal{L}_{v \rightarrow t} + \mathcal{L}_{t \rightarrow v} \quad (5)$$

256 The $\mathcal{L}_{\text{Di-VTC}}$ loss combines a visual-to-textual loss
 257 ($\mathcal{L}_{v \rightarrow t}$) and a textual-to-visual loss ($\mathcal{L}_{t \rightarrow v}$):

$$\mathcal{L}_{v \rightarrow t} = - \sum_{g \in B} \frac{1}{|\text{p}(g)|} \sum_{i \in \text{p}(g)} \log \frac{\exp(\hat{v}_g^\top \hat{t}_i / \tau)}{\sum_{h \in B} \exp(\hat{v}_g^\top \hat{t}_h / \tau)} \quad (6)$$

$$\mathcal{L}_{t \rightarrow v} = - \sum_{h \in B} \frac{1}{|\text{p}(h)|} \sum_{i \in \text{p}(h)} \log \frac{\exp(\hat{v}_i^\top \hat{t}_h / \tau)}{\sum_{g \in B} \exp(\hat{v}_i^\top \hat{t}_g / \tau)} \quad (7)$$

262 where $\text{p}(\cdot)$ denotes the set of positive pair indices
 263 for a given anchor sample, and τ is a temperature
 264 hyperparameter. The Di-VTC framework aligns
 265 visual and textual representations using similarity
 266 in predicted disease embeddings as supervision,
 267 enabling clinically grounded and coherent QA-style
 268 report generation.



269 Figure 3: Conceptual illustration of the Disease-aware
 270 Visual–Textual Contrast (Di-VTC) framework. The
 271 model optimizes a "push–pull" dynamic where pos-
 272 itive visual–textual pairs sharing disease labels (green
 273 lines) are pulled closer, while unrelated pairs (red lines)
 274 are pushed apart, strictly enforcing diagnostically con-
 275 sistent alignment in the shared embedding space.

2.3 STAGE 2: Knowledge-Guided QA-Style Report

276 **Intermediate Report Generation:** We generate
 277 the intermediate report R_I using a text decoder con-
 278 ditioned on the visual channel V_{ch} , textual chan-
 279 nel T_{ch} , and predicted diagnostic labels L_{ch} from
 280 STAGE 1. For each k^{th} study, the decoder produces
 281 a sequence that closely matches the ground-truth
 282 (GT) report $R_k = R_k^1, \dots, R_k^l$, where l is the report
 283 length. At each step t , it predicts token R_k^t
 284 conditioned upon all preceding tokens R_k^1, \dots, R_k^{t-1}
 285 and the integrated channel features (V_{ch}, T_{ch}, L_{ch}) .
 286 We employ the negative log-likelihood as the gen-
 287 eration loss \mathcal{L}_G to optimize the decoder:
 288

$$\mathcal{L}_G = - \sum_{t=1}^l \log p(R_k^t | R_k^1, \dots, R_k^{t-1}, V_{ch}, T_{ch}, L_{ch}) \quad (8)$$

289 where $p(R_k^t | \cdot)$ denotes the probability of gener-
 290 ating the t^{th} token given the preceding tokens and the
 291 multi-channel input. The loss \mathcal{L}_G ensures the
 292 decoder generates accurate clinically reports aligned
 293 with (V_{ch}, T_{ch}, L_{ch}) information.

294 **Knowledge Token Retrieval:** Unlike prior
 295 knowledge-injected RRG methods such as
 296 KiUT (Huang et al., 2023) and EKAGen (Bu
 297 et al., 2024a), which integrate external knowledge
 298 during decoding, CliQ-RRG integrates retrieved
 299 knowledge at the intermediate report level and
 300 utilizes LLM to restructure into QA-style pairs.
 301 Inspired by Liu et al. (2024a), we enrich the

intermediate report with external clinical knowledge to support QA-style synthesis. We construct a medical knowledge base $\mathcal{K}_{\text{ext}} = K_1, \dots, K_M$, where each K_m is a structured phrase describing a symptom, anatomical structure, or disease manifestation, curated from trusted online medical sources (refer Implementation Details). Inspired by the bootstrapping strategy in Liu et al. (2024a), we sample external documents relevant to the diagnostic labels $L_k = [l_k^{(i)}]_{i=1}^{14}$ obtained in STAGE 1, ensuring that the retrieved knowledge is clinically aligned. Using BioWordVec (Zhang et al., 2019b), we embed the intermediate report R_I and each knowledge entry K_m into a shared space \mathbb{R}^{d_w} , yielding vectors ϕ_{R_I} and ϕ_{K_m} . We then identify the top- k_t most relevant knowledge tokens by ranking them according to their cosine similarity with the report.

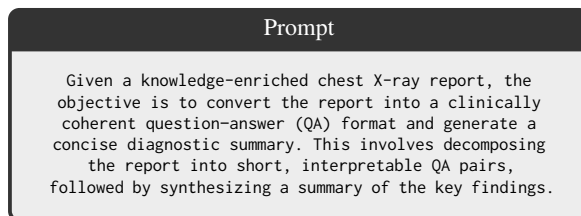
$$\text{sim}(\phi_{R_I}, \phi_{K_m}) = \frac{\phi_{R_I} \cdot \phi_{K_m}}{\|\phi_{R_I}\| \|\phi_{K_m}\|}, \forall m : 1 \rightarrow M \quad (9)$$

Next, we retrieve the indices of the top- k_t most relevant medical entries

$$\Lambda_{k_t} = \arg \max_{m \in [1, M]} \text{top-}k_t \text{ sim}(\phi_{R_I}, \phi_{K_m}) \quad (10)$$

Finally, the selected knowledge tokens $K_m | m \in \Lambda_{k_t}$ are appended to the intermediate report to create a knowledge-injected report, R_{KI} for the QA-style report generation.

QA-Style Report Generation: We employ *gpt-3.5-turbo* model from OpenAI, denoted as $\mathcal{G}(\cdot)$, to restructure the knowledge-injected report $R_{KI}^{(k)}$ into a set of clinically meaningful question–answer pairs $R_{qa}^{(k)}$ and a concise summary, where k indexes the study. A specific *Prompt* guides $\mathcal{G}(\cdot)$ to elicit the desired output format, as shown below:



We formalize the QA-style generation as:

$$R_{qa}^{(k)} = \mathcal{G}(R_{KI}^{(k)}, \text{Prompt}) \quad (11)$$

The output $R_{qa}^{(k)}$ contains m QA pairs, $\{(q_j, a_j)\}_{j=1}^m$, with q_j as the question and $a_j \in \{\text{Yes}, \text{No}\}$ as its concise answer. These are grouped thematically, with a final summary question encapsulating the key findings.

2.4 Learning Objective

We train the framework by jointly optimizing the disease-aware visual-textual contrastive, disease classification, and report generation objectives. The total loss is defined as:

$$\mathcal{L}_{\text{total}} = \mathcal{L}_{\text{Di-VTC}} + \lambda_1 \cdot \mathcal{L}_G + \lambda_2 \cdot \mathcal{L}_{\text{CE}} \quad (12)$$

where $\mathcal{L}_{\text{Di-VTC}}$ denotes the Disease-aware Visual-Textual Contrast loss, \mathcal{L}_{CE} is the disease classification loss computed using cross-entropy between predicted and CheXbert-derived labels, and \mathcal{L}_G represents the intermediate report generation loss. The coefficients λ_1 and λ_2 balance the contributions of the generative and classification objectives, and are empirically set to 1.0 for equal weighting.

3 Experimental Setting

Datasets: We evaluate CliQ-RRG on two public benchmarks: (1) MIMIC-CXR (Johnson et al., 2019), the largest RRG dataset with 337,110 scans and 227,835 reports, using the official train/validation/test split (Chen et al., 2020; Park et al., 2025); and (2) IU X-Ray (Demner-Fushman et al., 2015), a smaller set with 7,470 frontal and lateral scans and 3,955 reports, divided into 7:2:1 splits following prior work (Chen et al., 2020; Park et al., 2025).

Metrics: Following prior work (Jin et al., 2024; Park et al., 2025), we evaluate report quality using standard NLG metrics: BLEU (B) (Papineni et al., 2001), METEOR (MTR) (Denkowski and Lavie, 2011), ROUGE-L (RG-L) (Lin, 2004), and BERTScore (BERT) (Zhang et al., 2019a). For binary yes/no QA pairs, we follow recent studies (Manes et al., 2024; Kim et al., 2024) and conduct expert evaluation. Clinical Efficacy (CE) is assessed by labeling generated reports with CheXpert (Smit et al., 2020) and computing F1, Precision (Pre), and Recall (Rec). Inter-annotator agreement is measured using pairwise agreement and Fleiss' kappa (κ_F).

Implementation Details The framework is implemented in TensorFlow and trained on an NVIDIA Tesla T4 GPU using the AdamW optimizer (Loshchilov and Hutter, 2019). We train for 30 epochs with batch size 16, learning rate $3e-5$, and weight decay 0.01. At inference, the *gpt-3.5-turbo* is employed in a few-shot setting to restructure the knowledge-injected report into QA pairs without fine-tuning. Implementation details are provided in appendix D.

Table 1: Quantitative comparison of CliQ-RRG with SOTA methods on MIMIC-CXR and IU X-Ray. †: Results from published papers; *: Results reproduced from released code. **Bold**: best and underlined: second-best scores.

Type	Method	Published	MIMIC-CXR					IU X-Ray				
			B1	B4	MTR	RG-L	BERT [#]	B1	B4	MTR	RG-L	BERT [#]
I	R2GenRL* (Qin and Song, 2022)	ACL'22	0.392	0.113	0.149	0.275	0.852	0.487	0.177	0.205	0.377	0.835
	DCL* (Li et al., 2023)	CVPR'23	0.384	0.114	0.147	0.278	0.844	0.483	0.171	0.201	0.391	0.838
	MAN† (Shen et al., 2024)	AAAI'24	0.396	0.115	0.151	0.274	—	0.501	0.170	0.213	0.386	—
	CoFE* (Li et al., 2024a)	ECCV'24	0.393	0.133	0.172	0.316	0.860	0.406	0.177	0.199	0.423	0.849
	SEI* (Liu et al., 2024b)	MICCAI'24	0.381	0.119	0.148	0.306	0.841	0.486	0.173	0.209	0.395	0.837
	DART† (Park et al., 2025)	CVPR'25	0.437	0.137	0.175	0.310	—	0.486	0.208	0.205	0.411	—
II	KiUT† (Huang et al., 2023)	CVPR'23	0.393	0.113	0.160	0.285	—	0.525	0.185	0.242	0.409	—
	EKAGen† (Bu et al., 2024a)	CVPR'24	0.419	0.119	0.157	0.287	—	0.526	0.203	0.214	0.404	—
	PromptMRG† (Jin et al., 2024)	AAAI'24	0.398	0.112	0.157	0.268	—	0.401	0.098	0.160	0.281	—
	RADAR* (Hou et al., 2025)	ACL'25	0.493	<u>0.277</u>	0.170	0.304	<u>0.897</u>	0.411	0.119	0.171	0.293	0.840
III	REVTAF† (Zhou et al., 2025)	ICCV'25	0.465	0.182	0.199	0.336	—	0.420	0.107	0.176	0.309	—
	R2-LLM* (Liu et al., 2024a)	AAAI'24	0.411	0.132	0.179	0.288	0.873	0.487	0.178	0.215	0.401	0.846
	AdaMatch-Cyclic† (Chen et al., 2024)	ACL'24	0.379	0.101	0.163	0.286	—	0.416	0.145	0.162	0.366	—
	KARGEN† (Li et al., 2024b)	MICCAI'24	0.417	0.140	0.165	0.305	—	0.490	0.180	0.218	0.385	—
IV	LLM-RG4* (Wang et al., 2025)	AAAI'25	0.384	0.136	0.155	0.322	0.849	0.442	0.179	0.192	0.403	0.848
	MPO† (Xiao et al., 2025)	AAAI'25	0.416	0.139	0.162	0.309	—	0.548	0.209	0.224	0.415	—
	ORID† (Gu et al., 2025)	WACV'25	0.386	0.117	0.150	0.284	—	0.501	0.198	0.211	0.400	—
V	CoD† (Jin et al., 2025)	TMI'25	0.412	0.129	—	0.286	—	0.403	0.091	—	0.288	—
	CliQ-RRG (Knowledge-Injected)	Ours	<u>0.498</u>	0.275	0.182	0.324	<u>0.897</u>	<u>0.553</u>	<u>0.216</u>	0.221	<u>0.434</u>	<u>0.878</u>
	CliQ-RRG (QA Pair)	Ours	0.516	<u>0.284</u>	<u>0.191</u>	<u>0.343</u>	0.911	0.561	<u>0.227</u>	<u>0.230</u>	<u>0.442</u>	0.895

I: Contrastive-based; II: Knowledge Injected-based; III: LLM-based, IV: Multi View-based; V: QA Style-based # : BERT scores are reported for * methods using reproduced outputs; All reproduced methods use the same test set for fair comparison

Table 2: Comparison of CE metrics of CliQ-RRG on the MIMIC-CXR dataset. †: Results from published papers. **Bold**: best and underlined: second-best scores.

Method	Pre	Rec	F1
R2GenRL† (Qin and Song, 2022)	0.342	0.294	0.292
DCL† (Li et al., 2023)	0.471	0.352	0.373
MAN† (Shen et al., 2024)	0.411	0.398	0.389
CoFE† (Li et al., 2024a)	0.489	0.370	0.405
DART† (Park et al., 2025)	0.533	0.520	0.546
EKAGen† (Bu et al., 2024a)	0.517	0.483	0.499
PromptMRG† (Jin et al., 2024)	0.501	0.509	0.476
KiUT† (Huang et al., 2023)	0.371	0.318	0.321
REVTAF† (Zhou et al., 2025)	0.628	<u>0.613</u>	0.592
R2-LLM† (Liu et al., 2024a)	0.465	0.482	0.473
LLM-RG4† (Wang et al., 2025)	0.583	0.593	0.588
MPO† (Xiao et al., 2025)	0.436	0.376	0.353
ORID† (Gu et al., 2025)	0.435	0.295	0.352
CoD† (Jin et al., 2025)	0.487	0.521	0.479
CliQ-RRG (Knowledge-Injected)	0.591	0.602	<u>0.596</u>
CliQ-RRG (QA Pair)	0.605	0.618	0.611
Disease Classifier	0.496	0.515	0.505

4 Result and Discussion

Quantitative Analysis: We compare CliQ-RRG with five categories (Appendix B) on MIMIC-CXR and IU X-Ray. All reproduced baselines (*) follows original configurations (i.e., without prior scans and external knowledge). For fair comparison, we evaluate two settings: (i) Knowledge-Injected (R_{KI}), before QA restructuring, and (ii) QA-Pair (R_{qa}), which aggregates the diagnostic summary and generated QA-pairs into a single sequence and compares it with GT reports. Although the GT and QA-pair format differs, the diagnostic summary

and findings produce a high density of clinically relevant terms, ensures strong n -gram overlap and fair comparison with baselines. We further report format-independent metrics (BERTScore, CE) to verify diagnostic grounding improvements.

Comparison with State-of-the-Art Methods: As detailed in Table 1, CliQ-RRG achieves SOTA performance across most metrics. Compared to contrastive and LLM-based baselines, our framework demonstrates stronger semantic alignment with the GT. On the multi-view MIMIC-CXR and IU X-Ray datasets, CliQ-RRG outperforms all competitors, including MPO (Xiao et al., 2025), highlighting the effectiveness of the PrAM for multi-view integration. Knowledge-injected methods such as RADAR (Hou et al., 2025) on MIMIC-CXR and KiUT (Huang et al., 2023) on IU X-Ray remain competitive. REVTAF (Zhou et al., 2025) achieves the highest MTR and second-highest RG-L on MIMIC-CXR. We outperform CoD (Jin et al., 2025) QA-style baselines in both evaluation settings, confirming the efficacy of our tri-channel alignment and knowledge injection.

Evaluation of Clinical Efficacy Metrics: Table 2 reports CE metric on MIMIC-CXR, where CliQ-RRG achieves the superior performance and outperforms REVTAF (Zhou et al., 2025) in Pre. We also evaluate the disease classifier, confirming that classifier provides reliable supervisory signals to accurately guide multimodal alignment.

Table 3: Ablation analysis on MIMIC-CXR showing incremental performance gains by integrating the PrAM, Di-VTC (across V_{ch} - T_{ch} and L_{ch}), \mathcal{K}_{ext} , and LLM component into the base model. Results are reported as mean \pm std over five runs; * indicates statistically significant improvement over the base model ($p \leq 0.05$).

Model	STAGE 1			STAGE 2		NLG Metrics					CE Metrics			
	PrAM	V_{ch} - T_{ch}	L_{ch}	\mathcal{K}_{ext}	LLM	BL-1	BL-4	MTR	RG-L	∇_N	P	R	F1	∇_C
Base ^x	✗	✗	✗	✗	✗	0.381 \pm 0.004	0.185 \pm 0.005	0.157 \pm 0.003	0.295 \pm 0.004	—	0.455	0.471	0.463	—
(a)	✗	✓	✗	✗	✗	0.399 \pm 0.003	0.197 \pm 0.004	0.160 \pm 0.002	0.301 \pm 0.005	3.8%	0.472	0.493	0.482	4.2%
(b)	✓	✗	✗	✗	✗	0.404 \pm 0.005	0.208 \pm 0.006	0.163 \pm 0.003	0.302 \pm 0.004	5.8%	0.485	0.501	0.493	6.5%
(c)	✓	✓	✗	✗	✗	0.422 \pm 0.004	0.233 \pm 0.005	0.169 \pm 0.004	0.311 \pm 0.006	11.5%	0.498	0.519	0.508	9.8%
(d)	✗	✓	✓	✗	✗	0.442 \pm 0.006	0.224 \pm 0.004	0.169 \pm 0.003	0.309 \pm 0.005	12.4%	0.511	0.541	0.526	13.6%
(e)	✓	✓	✓	✗	✗	0.465 \pm 0.005	0.247 \pm 0.006	0.175 \pm 0.004	0.314 \pm 0.004	18.0%	0.542	0.565	0.553	19.5%
(f)	✗	✓	✓	✓	✗	0.472 \pm 0.004	0.256 \pm 0.005	0.178 \pm 0.003	0.319 \pm 0.006	20.3%	0.556	0.588	0.572	23.5%
(g) ^y	✓	✓	✓	✓	✗	0.498 \pm 0.005*	0.275 \pm 0.004*	0.182 \pm 0.004*	0.324 \pm 0.005*	25.6%	0.591	0.602	0.596	28.8%
(h) ^z	✓	✓	✓	✓	✓	0.516 \pm 0.003*	0.284 \pm 0.007*	0.191 \pm 0.005*	0.343 \pm 0.006*	31.0%	0.605	0.618	0.611	32.1%

PrAM: Prior-Guided Attention Module; V_{ch} : Visual Channel; T_{ch} : Textual Channel; L_{ch} : Predicted diagnostic label; \mathcal{K}_{ext} : External clinical knowledge.

LLM: Large Language Model; ∇_N and ∇_C : Average improvement over the base configuration for NLG and CE metrics;

x: CliQ-RRG (Base Model); y: CliQ-RRG (Knowledge-Injected); z: CliQ-RRG (QA Pair)



Figure 4: Qualitative analysis of CliQ-RRG on MIMIC-CXR. Report comparison across models given input and prior scans, with ground truth (GT). Shared medical terms use consistent color coding, and Grad-CAM highlights anatomically and pathologically relevant regions.

Ablation Study: We analyze the contribution of each component in CliQ-RRG on MIMIC-CXR (Table 3) and IU X-Ray (appendix E). The **base** model uses a visual encoder and transformer decoder, without alignment or knowledge injection. Integrating visual (V_{ch}) and textual (T_{ch}) channels (**model a**) yields marginal gains (B4: 0.197, F1: 0.482), showing the limitation of CLIP-style alignment. Conversely, adding PrAM to the base (**model b**) enhances clinical efficacy (F1: 0.493) by focusing on relevant regions. Combining both (**model c**) further improves the F1 to 0.508. Replacing CLIP-

style alignment with Di-VTC (**model d**), which aligns V_{ch} - T_{ch} - L_{ch} , yields stronger gains (B4: 0.224), demonstrates label-based grounding superior to image-text pairing. Integrating PrAM with Di-VTC (**model e**) improves NLG and CE metrics. Adding \mathcal{K}_{ext} into Di-VTC (**model f**) improves semantic completeness (F1: 0.572). The knowledge-enhanced framework (**model g**) outperforms the base model (NLG: +25.6%, CE: +28.8%), validating that \mathcal{K}_{ext} complements V_{ch} - T_{ch} - L_{ch} channel alignment. Our full framework with LLM-based QA restructuring (**model h**) attains the best perfor-

mance, with improvements of 31.0% (NLG) and 32.1% (CE). Results are reported as mean \pm std over five runs, and models (g) and (h) show statistically significant gains ($p \leq 0.05$).

Qualitative Analysis; Fig. 4 illustrates how each component of CliQ-RRG progressively enhances report quality on a MIMIC-CXR sample. The base model produces generic statements such as “*no acute abnormality*”, lacking clinical detail. Adding the *PrAM* introduces precise findings (“*no evidence of consolidation*”), while the *Disease-aware Visual–Textual Contrast* identifies key observations like “*focal consolidation, pleural effusion, or pneumothorax*”. Incorporating predicted disease embeddings improves diagnostic grounding, capturing terms such as “*cardiomegaly*”. Enriching the report with external clinical knowledge further refines phrasing (“*stable and unremarkable*”), aligning closely with the ground truth and enabling structured QA-style outputs. GradCAM (Selvaraju et al., 2017) visualizations confirm that CliQ-RRG focuses on relevant anatomical regions, validating anatomically grounded reasoning.

Parameter Sensitivity Analysis: We analyze the sensitivity of key hyperparameters λ_1 , λ_2 , and τ on MIMIC-CXR. As shown in Fig. 5, we vary $\lambda_1, \lambda_2 \in [0.5, 1.0, 1.5]$ and $\tau \in [0.03, 0.05, 0.07, 0.10]$ while keeping other parameters fixed. The method achieves optimal performance across all metrics when $\lambda_1 = \lambda_2 = 1.0$, indicating that equal weighting balances generation and classification objectives. Performance peaks at $\tau = 0.07$, suggesting an appropriate temperature for contrastive alignment.

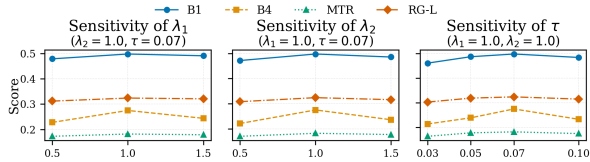


Figure 5: Parameter sensitivity analysis on MIMIC-CXR showing the effect of generation loss weight (λ_1), classification loss weight (λ_2), and temperature (τ).

Human Evaluation: We conduct a two-tier clinical validation to assess the reliability of the generated QA pairs. (i) We randomly sample 1,000 QA pairs generated by CliQ-RRG and evaluate using a standard Likert-scale protocol. Three medical professionals (2 doctors and 1 medical student) independently rate each QA pair against the ground-truth report on a 5-point scale across five criteria: overall quality, consistency, clinical relevance,

specificity, and fluency, following the rubric of Hashemi et al. (2024) (Table 4 (i)). We measure annotation reliability using Fleiss’ kappa (κ_F) and pairwise agreement (PA). (ii) To assess clinical accuracy and hallucination, we perform an independent clinical validation with a senior radiologist with over 20 years of experience. We select 200 QA pairs randomly from MIMIC-CXR and compare with corresponding GT reports, categorizing each pair as fully acceptable, clinically acceptable, or hallucinated. As shown in Table 4 (ii), 189 pairs are fully acceptable, and 9 are clinically consistent, yielding a 99.0% reliability rate, with 1.0% hallucinated content. The results validate that restructuring into a QA pair preserves diagnostic correctness.

Table 4: Human evaluation of generated QA pairs: (i) 5-point Likert ratings (R_0-R_4) with inter-annotator agreement; (ii) independent clinical assessment of QA integrity and hallucinations against ground truth.

	Dataset	R_0	R_1	R_2	R_3	R_4	PA	κ_F
(i)	MIMIC-CXR	4.03	3.96	4.25	4.09	4.23	0.79	0.76
	IU X-Ray	4.13	4.09	4.43	3.91	4.11	0.82	0.78
Outcome							Count	%
(ii)	Fully acceptable							189 94.5%
	Clinically acceptable (minor linguistic deviations)							9 4.5%
	Hallucinated (contradictory/unsupported findings)							2 1.0%
	Total Reliable (Fully + Clinically) Pairs							198 99.0%

5 Related Work

Due to space constraints in the main text, we provide a comprehensive discussion of related work and prior approaches in Appendix A.

6 Conclusion

In this paper, we present CliQ-RRG, for QA-style radiology report generation. CliQ-RRG introduces a disease-aware visual–textual contrastive scheme to align visual, textual, and predicted diagnostic labels, enhanced by a prior-guided attention for integrating multi-view chest X-rays. Additionally, injecting domain-specific clinical information enriches the semantic depth of the generated reports and supports the structured QA formulation. Qualitative analysis shows that CliQ-RRG effectively aligns the visual, textual, and label modalities to generate clinically reliable QA-style radiology reports. Experiments on MIMIC-CXR and IU X-Ray benchmarks highlight the superiority of our proposed framework over state-of-the-art methods.

530 7 Limitations

531 While CliQ-RRG demonstrates strong performance,
532 several limitations suggest directions for
533 future improvement. First, the QA formulation is
534 grounded in a predefined diagnostic label space
(i.e., CheXpert categories), which ensures systematic
535 coverage of clinically important findings but
536 may limit open-set detection of rare or previously
537 unseen diseases. Second, the current study focuses
538 on 2D CXR modalities, which enable a controlled
539 analysis of disease-aware alignment and QA-style
540 reporting but do not cover modalities with richer
541 spatial structure. Third, the large language model is
542 used as a fixed restructuring component to convert
543 knowledge-enriched reports into structured yes or
544 no QA pairs, rather than being jointly optimized
545 for multimodal reasoning. Fourth, evaluation is
546 limited to MIMIC-CXR and IU X-Ray, which follow
547 specific acquisition protocols and population
548 characteristics. Fifth, the framework relies on supervised
549 learning with paired images, reports, and
550 diagnostic labels, which may constrain scalability
551 in data-scarce settings. Finally, external knowledge
552 is retrieved through semantic similarity, prioritizing
553 accurate grounding while leaving explicit modeling
554 of disease interdependencies unaddressed.

556 References

- 557 Josh Achiam, Steven Adler, Sandhini Agarwal, Lama
558 Ahmad, Ilge Akkaya, Florencia Leoni Aleman,
559 Diogo Almeida, Janko Altenschmidt, Sam Altman,
560 Shyamal Anadkat, and 1 others. 2023. Gpt-4 technical
561 report. *arXiv preprint arXiv:2303.08774*.
- 562 Benedikt Boecking, Naoto Usuyama, Shruthi Bannur,
563 Daniel C. Castro, Anton Schwaighofer, Stephanie
564 Hyland, Maria Wetscherek, Tristan Naumann, Aditya
565 Nori, Javier Alvarez-Valle, Hoifung Poon, and Ozan
566 Oktay. 2022. Making the most of text semantics to
567 improve biomedical vision-language processing. In
568 *European conference on computer vision*, volume
569 13696 LNCS, pages 1–21.
- 570 Shenshen Bu, Taiji Li, and Zhiming Dai. 2023. Enhanc-
571 ing medical report generation in multi-slice fusion
572 scenarios. In *2023 IEEE International Conference
573 on Bioinformatics and Biomedicine (BIBM)*, page
574 1030–1037. IEEE.
- 575 Shenshen Bu, Taiji Li, Yuedong Yang, and Zhiming
576 Dai. 2024a. Instance-level expert knowledge and ag-
577 gregate discriminative attention for radiology report
578 generation. In *2024 IEEE/CVF Conference on Com-
579 puter Vision and Pattern Recognition (CVPR)*, page
580 14194–14204. IEEE.

- 581 Shenshen Bu, Yujie Song, Taiji Li, and Zhiming Dai.
582 2024b. Dynamic knowledge prompt for chest x-ray
583 report generation. In *Proceedings of the 2024 Joint
584 International Conference on Computational Linguis-
585 tics, Language Resources and Evaluation (LREC-
586 COLING 2024)*, pages 5425–5436.
- 587 Wenting Chen, Linlin Shen, Jingyang Lin, Jiebo Luo,
588 Xiang Li, and Yixuan Yuan. 2024. Fine-grained
589 image-text alignment in medical imaging enables
590 explainable cyclic image-report generation. In *Pro-
591 ceedings of the 62nd Annual Meeting of the Associa-
592 tion for Computational Linguistics (Volume 1: Long
593 Papers)*, page 9494–9509. Association for Compu-
594 tational Linguistics.
- 595 Zhihong Chen, Yaling Shen, Yan Song, and Xiang Wan.
596 2021. Cross-modal memory networks for radiology
597 report generation. In *Proceedings of the 59th Annual
598 Meeting of the Association for Computational Lin-
599 guistics and the 11th International Joint Conference
600 on Natural Language Processing (Volume 1: Long
601 Papers)*. Association for Computational Linguistics.
- 602 Zhihong Chen, Yan Song, Tsung-Hui Chang, and Xi-
603 ang Wan. 2020. Generating radiology reports via
604 memory-driven transformer. In *Proceedings of the
605 2020 Conference on Empirical Methods in Natu-
606 ral Language Processing (EMNLP)*. Association for
607 Computational Linguistics.
- 608 Dina Demner-Fushman, Marc D. Kohli, Marc B. Rosen-
609 man, Sonya E. Shooshan, Laritza Rodriguez, Sameer
610 Antani, George R. Thoma, and Clement J. McDon-
611 ald. 2015. Preparing a collection of radiology ex-
612 aminations for distribution and retrieval. *Journal
613 of the American Medical Informatics Association*,
614 23(2):304–310.
- 615 Michael Denkowski and Alon Lavie. 2011. Meteor 1.3:
616 Automatic metric for reliable optimization and evalua-
617 tion of machine translation systems. In *WMT 2011
618 - 6th Workshop on Statistical Machine Translation,
619 Proceedings of the Workshop*, pages 85–91.
- 620 Aaron Grattafiori, Abhimanyu Dubey, Abhinav Jauhri,
621 Abhinav Pandey, Abhishek Kadian, Ahmad Al-
622 Dahle, Aiesha Letman, Akhil Mathur, Alan Schelten,
623 Alex Vaughan, and 1 others. 2024. The llama 3 herd
624 of models. *arXiv preprint arXiv:2407.21783*.
- 625 Tiancheng Gu, Dongnan Liu, Zhiyuan Li, and Weidong
626 Cai. 2024. Complex organ mask guided radiology
627 report generation. In *2024 IEEE/CVF Winter Con-
628 ference on Applications of Computer Vision (WACV)*,
629 page 7980–7989. IEEE.
- 630 Tiancheng Gu, Kaicheng Yang, Xiang An, Ziyong Feng,
631 Dongnan Lin, and Weidong Cai. 2025. Orid: Organ-
632 regional information driven framework for radiology
633 report generation. In *2025 IEEE/CVF Winter Con-
634 ference on Applications of Computer Vision (WACV)*,
635 page 378–387. IEEE.
- 636 Helia Hashemi, Jason Eisner, Corby Rosset, Benjamin
637 Van Durme, and Chris Kedzie. 2024. Llm-rubric: A

638	multidimensional, calibrated approach to automated evaluation of natural language texts. In <i>Proceedings of the 62nd Annual Meeting of the Association for Computational Linguistics (Volume 1: Long Papers)</i> , page 13806–13834. Association for Computational Linguistics.	695
639		696
640		
641		
642		
643		
644	Wenjun Hou, Yi Cheng, Kaishuai Xu, Heng Li, Yan Hu, Wenjie Li, and Jiang Liu. 2025. Radar: Enhancing radiology report generation with supplementary knowledge injection . In <i>Proceedings of the 63rd Annual Meeting of the Association for Computational Linguistics (Volume 1: Long Papers)</i> , pages 26366–26381. Association for Computational Linguistics.	697
645		698
646		
647		
648		
649		
650		
651	Wenjun Hou, Kaishuai Xu, Yi Cheng, Wenjie Li, and Jiang Liu. 2023. Organ: Observation-guided radiology report generation via tree reasoning . In <i>Proceedings of the 61st Annual Meeting of the Association for Computational Linguistics (Volume 1: Long Papers)</i> . Association for Computational Linguistics.	703
652		704
653		
654		
655		
656		
657	Xiyang Huang, Yingjie Han, Yx L, Runzhi Li, Pengcheng Wu, and Kunli Zhang. 2025. CmEAA: Cross-modal enhancement and alignment adapter for radiology report generation . In <i>Proceedings of the 31st International Conference on Computational Linguistics</i> , pages 8546–8556. Association for Computational Linguistics.	705
658		706
659		
660		
661		
662		
663		
664	Zhongzhen Huang, Xiaofan Zhang, and Shaoting Zhang. 2023. Kiut: Knowledge-injected u-transformer for radiology report generation . In <i>2023 IEEE/CVF Conference on Computer Vision and Pattern Recognition (CVPR)</i> , page 19809–19818. IEEE.	707
665		708
666		
667		
668		
669	Haibo Jin, Haoxuan Che, Sunan He, and Hao Chen. 2025. A chain of diagnosis framework for accurate and explainable radiology report generation . <i>IEEE Transactions on Medical Imaging</i> , 44(12):4986–4997.	709
670		
671		
672		
673		
674	Haibo Jin, Haoxuan Che, Yi Lin, and Hao Chen. 2024. Promptmrg: Diagnosis-driven prompts for medical report generation . <i>Proceedings of the AAAI Conference on Artificial Intelligence</i> , 38(3):2607–2615.	710
675		711
676		
677		
678	Alistair E. W. Johnson, Tom J. Pollard, Nathaniel R. Greenbaum, Matthew P. Lungren, Chih ying Deng, Yifan Peng, Zhiyong Lu, Roger G. Mark, Seth J. Berkowitz, and Steven Horng. 2019. Mimic-cxr-jpg, a large publicly available database of labeled chest radiographs . <i>Preprint</i> , arXiv:1901.07042.	712
679		713
680		
681		
682		
683		
684	Gregory Kell, Angus Roberts, Serge Umansky, Linglong Qian, Davide Ferrari, Frank Soboczenski, Byron C Wallace, Nikhil Patel, and Iain J Marshall. 2024. Question answering systems for health professionals at the point of care—a systematic review . <i>Journal of the American Medical Informatics Association</i> , 31(4):1009–1024.	714
685		715
686		
687		
688		
689		
690		
691	Yunsoo Kim, Jing Wu, Yusuf Abdulle, and Honghan Wu. 2024. Medexqa: Medical question answering benchmark with multiple explanations . In <i>Proceedings of the 23rd Workshop on Biomedical Natural</i>	716
692		717
693		
694		
695	<i>Language Processing</i> , page 167–181. Association for Computational Linguistics.	718
696		719
697		
698		
699		
700		
701		
702		
703	Mingjie Li, Bingqian Lin, Zicong Chen, Haokun Lin, Xiaodan Liang, and Xiaojun Chang. 2023. Dynamic graph enhanced contrastive learning for chest x-ray report generation . In <i>2023 IEEE/CVF Conference on Computer Vision and Pattern Recognition (CVPR)</i> , page 3334–3343. IEEE.	720
704		721
705		
706		
707		
708		
709		
710	Mingjie Li, Haokun Lin, Liang Qiu, Xiaodan Liang, Ling Chen, Abdulmotaleb Elsaddik, and Xiaojun Chang. 2024a. Contrastive learning with counterfactual explanations for radiology report generation . In <i>Proceedings of the European Conference on Computer Vision (ECCV)</i> , pages 162–180. Springer Nature Switzerland.	722
711		723
712		
713		
714		
715	Yingshu Li, Zhanyu Wang, Yunyi Liu, Lei Wang, Lingqiao Liu, and Luping Zhou. 2024b. KARGEN: Knowledge-Enhanced Automated Radiology Report Generation Using Large Language Models , page 382–392. Springer Nature Switzerland.	724
716		725
717		
718		
719		
720		
721		
722	Xiao Liang, Yanlei Zhang, Di Wang, Haodi Zhong, Ronghan Li, and Quan Wang. 2024. Divide and conquer: Isolating normal-abnormal attributes in knowledge graph-enhanced radiology report generation . In <i>Proceedings of the 32nd ACM International Conference on Multimedia, MM ’24</i> , page 4967–4975. ACM.	726
723		727
724		
725	Chin-Yew Lin. 2004. Rouge: A package for automatic evaluation of summaries . In <i>Text summarization branches out</i> , pages 74–81.	728
726		729
727		
728		
729		
730	Qika Lin, Kai He, Yifan Zhu, Fangzhi Xu, Erik Cambria, and Mengling Feng. 2025. Cross-modal knowledge diffusion-based generation for difference-aware medical vqa . <i>IEEE Transactions on Image Processing</i> , 34:2421–2434.	731
731		732
732		
733		
734		
735	Chang Liu, Yuanhe Tian, Weidong Chen, Yan Song, and Yongdong Zhang. 2024a. Bootstrapping large language models for radiology report generation . <i>Proceedings of the AAAI Conference on Artificial Intelligence</i> , 38(17):18635–18643.	736
736		737
737		
738		
739		
740		
741	Kang Liu, Zhuoqi Ma, Xiaolu Kang, Yunan Li, Kun Xie, Zhicheng Jiao, and Qiguang Miao. 2025a. Enhanced contrastive learning with multi-view longitudinal data for chest x-ray report generation. In <i>Proceedings of the Computer Vision and Pattern Recognition Conference (CVPR)</i> , pages 10348–10359.	742
742		743
743		
744		
745		
746		
747	Kang Liu, Zhuoqi Ma, Xiaolu Kang, Zhusi Zhong, Zhicheng Jiao, Grayson Baird, Harrison Bai, and Qiguang Miao. 2024b. Structural Entities Extraction and Patient Indications Incorporation for Chest X-Ray Report Generation , page 433–443. Springer Nature Switzerland.	748
748		749
749		
750		
751		

752	Tengfei Liu, Jiapu Wang, Yongli Hu, Mingjie Li, Junfei Yi, Xiaojun Chang, Junbin Gao, and Baocai Yin.	Lawrence H. Schwartz, David M. Panicek, Alexandra R. Berk, Yuelin Li, and Hedvig Hricak.	807
753	2025b. <i>Hc-lm: Historical-constrained large language models for radiology report generation</i> . <i>Proceedings of the AAAI Conference on Artificial Intelligence</i> , 39(6):5595–5603.	<i>Improving communication of diagnostic radiology findings through structured reporting</i> . <i>Radiology</i> , 260(1):174–181.	808
754			809
755			810
756			811
757			
758	Ilya Loshchilov and Frank Hutter. 2019. Decoupled weight decay regularization. In <i>7th International Conference on Learning Representations, ICLR 2019</i> .	Ramprasaath R. Selvaraju, Michael Cogswell, Abhishek Das, Ramakrishna Vedantam, Devi Parikh, and Dhruv Batra. 2017. <i>Grad-cam: Visual explanations from deep networks via gradient-based localization</i> . In <i>2017 IEEE International Conference on Computer Vision (ICCV)</i> , page 618–626. IEEE.	812
759			813
760			814
761			815
762	Jiasen Lu, Caiming Xiong, Devi Parikh, and Richard Socher. 2017. <i>Knowing when to look: Adaptive attention via a visual sentinel for image captioning</i> . In <i>2017 IEEE Conference on Computer Vision and Pattern Recognition (CVPR)</i> . IEEE.	Hongyu Shen, Mingtao Pei, Juncai Liu, and Zhaoxing Tian. 2024. <i>Automatic radiology reports generation via memory alignment network</i> . <i>Proceedings of the AAAI Conference on Artificial Intelligence</i> , 38(5):4776–4783.	816
763			817
764			
765			
766			
767	Yuanjiang Luo, Hongxiang Li, Xuan Wu, Meng Cao, Xiaoshuang Huang, Zhihong Zhu, Peixi Liao, Hu Chen, and Yi Zhang. 2024. <i>Textual Inversion and Self-supervised Refinement for Radiology Report Generation</i> , page 681–691. Springer Nature Switzerland.	Akshay Smit, Saahil Jain, Pranav Rajpurkar, Anuj Parereek, Andrew Ng, and Matthew Lungren. 2020. <i>Combining automatic labelers and expert annotations for accurate radiology report labeling using bert</i> . In <i>Proceedings of the 2020 Conference on Empirical Methods in Natural Language Processing (EMNLP)</i> . Association for Computational Linguistics.	818
768			819
769			820
770			821
771			822
772	Itay Manes, Naama Ronn, David Cohen, Ran Ilan Ber, Zehavi Horowitz-Kugler, and Gabriel Stanovsky. 2024. <i>K-qa: A real-world medical q&a a benchmark</i> . In <i>Proceedings of the 23rd Workshop on Biomedical Natural Language Processing</i> , page 277–294. Association for Computational Linguistics.	Liwen Sun, James Jialun Zhao, Wenjing Han, and Chenyan Xiong. 2025. <i>Fact-aware multimodal retrieval augmentation for accurate medical radiology report generation</i> . In <i>Proceedings of the 2025 Conference of the Nations of the Americas Chapter of the Association for Computational Linguistics: Human Language Technologies (Volume 1: Long Papers)</i> , page 643–655. Association for Computational Linguistics.	823
773			824
774			825
775			826
776			827
777			828
778	Luis-Jesus Marhuenda, Miquel Obrador-Reina, Mohamed Aas-Alas, Alberto Albiol, and Roberto Paredes. 2025. Unveiling differences: A vision encoder-decoder model for difference medical visual question answering. In <i>Medical Imaging with Deep Learning</i> .	Gemini Team, Rohan Anil, Sebastian Borgeaud, Jean-Baptiste Alayrac, Jiahui Yu, Radu Soricut, Johan Schalkwyk, Andrew M Dai, Anja Hauth, Katie Millican, and 1 others. 2023. Gemini: a family of highly capable multimodal models. <i>arXiv preprint arXiv:2312.11805</i> .	829
779			
780			
781			
782			
783	Kishore Papineni, Salim Roukos, Todd Ward, and Wei-Jing Zhu. 2001. <i>Bleu: a method for automatic evaluation of machine translation</i> . In <i>Proceedings of the 40th Annual Meeting on Association for Computational Linguistics - ACL '02, ACL '02</i> , page 311. Association for Computational Linguistics.	Ashish Vaswani, Noam Shazeer, Niki Parmar, Jakob Uszkoreit, Llion Jones, Aidan N. Gomez, Łukasz Kaiser, and Illia Polosukhin. 2017. Attention is all you need. In <i>Advances in Neural Information Processing Systems</i> , volume 2017-December.	830
784			831
785			832
786			833
787			834
788			835
789	Sang-Jun Park, Keun-Soo Heo, Dong-Hee Shin, Young-Han Son, Ji-Hye Oh, and Tae-Eui Kam. 2025. Dart: Disease-aware image-text alignment and self-correcting re-alignment for trustworthy radiology report generation. In <i>Proceedings of the Computer Vision and Pattern Recognition Conference (CVPR)</i> , pages 15580–15589.	Zhuohao Wang, Yihua Sun, Zihan Li, Xuan Yang, Fang Chen, and Hongen Liao. 2025. <i>Llm-rg4: Flexible and factual radiology report generation across diverse input contexts</i> . <i>Proceedings of the AAAI Conference on Artificial Intelligence</i> , 39(8):8250–8258.	836
790			837
791			838
792			
793			
794			
795			
796	Priyaranjan Pattnayak, Hitesh Patel, Amit Agarwal, Srikant Panda, Bhargava Kumar, and Tejaswini Kumar. 2025. <i>Clinical qa 2.0- multi-task learning for answer extraction and categorization</i> . In <i>2025 IEEE International Conference on Electro Information Technology (eIT)</i> , page 1–7. IEEE.	Ting Xiao, Lei Shi, Peng Liu, Zhe Wang, and Chen-jia Bai. 2025. <i>Radiology report generation via multi-objective preference optimization</i> . <i>Proceedings of the AAAI Conference on Artificial Intelligence</i> , 39(8):8664–8672.	845
797			846
798			847
799			848
800			849
801			
802	Han Qin and Yan Song. 2022. <i>Reinforced cross-modal alignment for radiology report generation</i> . In <i>Findings of the Association for Computational Linguistics: ACL 2022</i> . Association for Computational Linguistics.	Kelvin Xu, Jimmy Lei Ba, Ryan Kiros, Kyunghyun Cho, Aaron Courville, Ruslan Salakhutdinov, Richard S. Zemel, and Yoshua Bengio. 2015. Show, attend and tell: Neural image caption generation with visual	850
803			851
804			852
805			853
806			854

864	attention. In <i>32nd International Conference on Machine Learning, ICML 2015</i> , volume 3, pages 2048–2057.		
865			
866			
867	Benjamin Yan, Ruochen Liu, David Kuo, Subathra Adithan, Eduardo Reis, Stephen Kwak, Vasantha Venugopal, Chloe O’Connell, Agustina Saenz, Pranav Rajpurkar, and Michael Moor. 2023. Style-aware radiology report generation with radgraph and few-shot prompting. In <i>Findings of the Association for Computational Linguistics: EMNLP 2023</i> , page 14676–14688. Association for Computational Linguistics.	LLM Choice on QA	Appendix F
868			
869			
870			
871			
872			
873			
874			
875			
876	Bin Yan and Mingtao Pei. 2022. Clinical-bert: Vision-language pre-training for radiograph diagnosis and reports generation. In <i>Proceedings of the AAAI conference on artificial intelligence</i> , volume 36, pages 2982–2990.	Computational Efficiency	Appendix G
877			
878			
879			
880			
881	Shuxin Yang, Xian Wu, Shen Ge, Zhuozhao Zheng, S Kevin Zhou, and Li Xiao. 2023. Radiology report generation with a learned knowledge base and multi-modal alignment. <i>Medical Image Analysis</i> , 86:102798.	Future Work	Appendix I
882			
883			
884			
885			
886	Sheng Zhang, Yanbo Xu, Naoto Usuyama, Hanwen Xu, Jaspreet Bagga, Robert Tinn, Sam Preston, Rajesh Rao, Mu Wei, Naveen Valluri, Cliff Wong, Andrea Tupini, Yu Wang, Matt Mazzola, Swadheen Shukla, Lars Liden, Jianfeng Gao, Angela Crabtree, Brian Piening, and 5 others. 2025. A multimodal biomedical foundation model trained from fifteen million image–text pairs. <i>NEJM AI</i> , 2(1).	Practical Implication	Appendix H
887			
888			
889			
890			
891			
892			
893			
894	Tianyi Zhang, Varsha Kishore, Felix Wu, Kilian Q Weinberger, and Yoav Artzi. 2019a. Bertscore: Evaluating text generation with bert. <i>arXiv preprint arXiv:1904.09675</i> .	Future Work	Appendix I
895			
896			
897			
898	Yijia Zhang, Qingyu Chen, Zhihao Yang, Hongfei Lin, and Zhiyong Lu. 2019b. Biowordvec, improving biomedical word embeddings with subword information and mesh. <i>Scientific Data</i> , 6(1).	Reproducibility	Appendix J
899			
900			
901			
902	Yixiao Zhang, Xiaosong Wang, Ziyue Xu, Qihang Yu, Alan Yuille, and Daguang Xu. 2020. When radiology report generation meets knowledge graph. In <i>Proceedings of the AAAI conference on artificial intelligence</i> , volume 34, pages 12910–12917.	LLM Choice on QA	Appendix F
903			
904			
905			
906			
907	Qin Zhou, Guoyan Liang, Xindi Li, Jingyuan Chen, Zhe Wang, Chang Yao, and Sai Wu. 2025. Learnable retrieval enhanced visual-text alignment and fusion for radiology report generation. In <i>Proceedings of the IEEE/CVF International Conference on Computer Vision</i> , pages 22529–22538.	Computational Efficiency	Appendix G
908			
909			
910			
911			
912			
913	Appendix		
914	Related Work	Appendix A	
915	Compared Baselines	Appendix B	
916	Knowledge Base Construction	Appendix C	
917	Implementation Details	Appendix D	
918	Ablation Results (IU dataset)	Appendix E	
919	LLM Choice on QA	Appendix F	
920	Computational Efficiency	Appendix G	
921	Future Work	Appendix I	
922	Practical Implication	Appendix H	
923	Future Work	Appendix I	
924	Reproducibility	Appendix J	
925	A Related Work		
926			
927	Encoder–Decoder and Multi-View RRG:		
928	Early RRG methods rely on encoder-decoder architectures to generate natural language descriptions from visual inputs (Xu et al., 2015; Lu et al., 2017; Chen et al., 2020). To better capture spatial and anatomical details, recent models incorporate multi-view X-rays and multi-slice features (Chen et al., 2021; Bu et al., 2023). For longitudinal tracking, HC-LLM (Liu et al., 2025b) uses historical constraints to guide large language models in generating progression-aware reports.		
929			
930			
931			
932			
933			
934			
935			
936			
937			
938	Contrastive Alignment:		
939	Multimodal contrastive learning is widely used to improve visual-textual alignment, ranging from global image-report matching to fine-grained region-word pairs (Li et al., 2023; Shen et al., 2024; Huang et al., 2025). Models like PromptMRG (Jin et al., 2024) use diagnostic labels as soft prompts to guide generation, while other methods integrate learned knowledge bases (Yang et al., 2023). AdaMatch-Cyclic (Chen et al., 2024) applies fine-grained cyclic alignment between image regions and text.		
940			
941			
942			
943			
944			
945			
946			
947			
948			
949			
950			
951	Knowledge-Injected Generation:		
952	Recent works inject external clinical knowledge into the generation process via attention mechanisms and knowledge graphs (Hou et al., 2025; Sun et al., 2025; Liu et al., 2024a). Notably, REVTAF (Zhou et al., 2025) fuses modal alignment and knowledge injection using a learnable retrieval enhancer in hyperbolic space and optimal transport-based cross-attention. Similarly, KiUT (Huang et al., 2023) integrates symptom graphs into a U-Transformer. Other approaches, like EKAGen (Bu et al., 2024a), retrieve instance-level expert knowledge and highlight key pathological regions, while DKP (Bu et al., 2024b) generates dynamic knowledge prompts from anomaly-driven features.		
953			
954			
955			
956			
957			
958			
959			
960			
961			
962			
963			
964			
965			
966			

967 **QA-Style Generation:** Motivated by limitations
 968 of narrative reporting (Jin et al., 2024; Luo et al.,
 969 2024; Wang et al., 2025; Kell et al., 2024; Pattnayak
 970 et al., 2025; Schwartz et al., 2011), limited clinical
 971 grounding (Yan et al., 2023; Bu et al., 2024a;
 972 Gu et al., 2024), underuse of diagnostic labels (Li
 973 et al., 2023; Shen et al., 2024; Xiao et al., 2025),
 974 and limited temporal fusion (Hou et al., 2023; Gu
 975 et al., 2025), recent work explores structured and
 976 explainable outputs. For example, CoD (Jin et al.,
 977 2025) prompts LLMs using findings extracted from
 978 diagnostic QA pairs. In medical VQA, MENDER
 979 (Lin et al., 2025) leverages cross-modal knowledge
 980 diffusion to achieve accurate answering. VED
 981 (Marhuenda et al., 2025) uses a vision encoder-
 982 decoder to detect and explain radiological changes
 983 across longitudinal X-rays.

985 **Summary:** Despite progress in alignment,
 986 knowledge injection, and QA formatting, prior
 987 works largely overlook longitudinal priors for
 988 structured reporting. CliQ-RRG addresses this
 989 by unifying disease-aware contrastive alignment
 990 with staged knowledge retrieval. Finally, it
 991 uses multi-view priors and employs an LLM to
 992 restructure standard narrative reports into precise,
 993 clinically meaningful QA-style outputs.

994 B Compared Baselines

995 We benchmark our proposed CliQ-RRG against
 996 state-of-the-art baselines, which we classify into
 997 five categories.

998 I: Contrastive-based Methods

- 999 • *R2GenRL* (Qin and Song, 2022) optimizes the
 1000 mapping between visual regions and textual
 1001 words using reinforcement learning based on
 1002 generation metrics.
- 1003 • *DCL* (Li et al., 2023) constructs dynamic relation
 1004 graphs and applies contrastive learning to
 1005 align visual features with medical entities.
- 1006 • *MAN* (Shen et al., 2024) uses a shared memory
 1007 mechanism to capture cross-modal correspondence
 1008 and guide attention during decoding.
- 1009 • *CoFE* (Li et al., 2024a) aligns representations
 1010 via contrastive learning that maximize similarity
 1011 for factual pairs while repelling negatives.
- 1012 • *SEI* (Liu et al., 2024b) aligns extracted
 1013 anatomical entities and patient indications
 1014 with corresponding visual regions.

- *DART* (Park et al., 2025) leverages diagnostic labels to ground text generation and incorporates a self-correcting mechanism to refine image-text consistency.

II: Knowledge Injected-based Methods

- *KiUT* (Huang et al., 2023) integrates clinical knowledge into a U-Transformer architecture using a symptom graph and an adaptive distiller to guide word prediction.
- *EKAGen* (Bu et al., 2024a) enhances generation by combining expert knowledge with discriminative attention mechanism to focus on pathological regions.
- *PromptMRG* (Jin et al., 2024) converts disease predictions into soft prompts and retrieves similar reports as in-context guidance.
- *RADAR* (Hou et al., 2025) injects external clinical knowledge and aligns it with visual features to enhance report reliability.
- *REVTAF* (Zhou et al., 2025) utilizes semantic hierarchy in hyperbolic space to get reference reports to improve clinical findings.

III: LLM-based Methods

- *R2-LLM* (Liu et al., 2024a) frames report generation as instruction following using a frozen LLM guided by visual prompts.
- *AdaMatch-Cyclic* (Chen et al., 2024) employs a cyclic framework with adaptive patch-word alignment to guide both report generation and image synthesis.
- *KARGEN* (Li et al., 2024b) integrates a medical knowledge graph with a frozen LLM to generate disease-sensitive reports.
- *LLM-RG4* (Wang et al., 2025) supports diverse input scenarios through adaptive token fusion and loss reweighting to reduce hallucinations.

IV: Multi View-based Methods

- *MPO* (Xiao et al., 2025) adapts report generation to different user preferences by optimizing weighted objectives through reinforcement learning.
- *ORID* (Gu et al., 2025) filters irrelevant noise using an instruction-tuned LLaVA-Med model to generate organ-specific descriptions prioritized by graph-based analysis.

V: QA Style-based Method

- 1062 • *CoD* (Jin et al., 2025) improves clinical ac-
 1063 curacy by generating QA pairs through a dia-
 1064 gnostic conversation framework to guide a
 1065 large language model during RRG.

1066 C Medical Knowledge Base Construction

1067 We construct an external knowledge base $\mathcal{K}_{ext} =$
 1068 $\{K_m\}_{m=1}^M$ for knowledge-guided generation used
 1069 in STAGE 2.

1070 Step 1: Source Collection

1071 We curated approximately 5,000 reliable medical
 1072 documents from PubMed abstracts related to tho-
 1073 racic imaging and chest radiology. Documents
 1074 were filtered to retain content relevant to radio-
 1075 graphic findings, disease descriptions, and anatomical
 1076 structures.

1077 Step 2: Knowledge Unit Extraction

1078 We processed the raw text to extract atomic clinical
 1079 facts rather than full paragraphs. Using a biomedical
 1080 Named Entity Recognition (NER) model in-
 1081 stantiated with BioClinicalBERT, we identified
 1082 sentences containing at least one radiology-relevant
 1083 entity (e.g., symptom, anatomical region, imaging
 1084 finding). Each sentence is converted into a concise
 1085 atomic phrase through normalization. The normal-
 1086 ization step removes redundant modifiers, standard-
 1087 izes terminology, and retains clinically meaningful
 1088 descriptors. Near-duplicate entries are filtered us-
 1089 ing cosine similarity thresholding.

1090 Step 3: Label Mapping

1091 Each knowledge entry \mathcal{K}_m is mapped to disease
 1092 category $y_m \in \mathcal{Y}$. This mapping ensures that the re-
 1093 trieval knowledge is consistent with the predicted
 1094 diagnostic labels (L_{ch}) used during the generation
 1095 process.

1096 Step 4: Embedding and Retrieval Setup

1097 We embedded each knowledge entry \mathcal{K}_m into a vec-
 1098 tor space using BioWordVec to create a searchable
 1099 index. During the report generation phase, we cal-
 1100 culate the cosine similarity between the embedding
 1101 of the generated intermediate report (ϕ_{R_I}) and the
 1102 knowledge entries (ϕ_{K_m}) to retrieve the top- k most
 1103 relevant clinical facts, which are then appended to
 1104 the report context.

1105 D Implementation Details

1106 Input CXRs are resized and cropped to $224 \times$
 1107 224 pixels. In STAGE 1, visual and textual en-
 1108 coder outputs are projected to $d_e = 768$ through
 1109 a linear layer, while STAGE 2 utilizes a Trans-
 1110 former (Vaswani et al., 2017) decoder with 8 at-

tention heads and a hidden size of 256. The genera-
 1111 tion length for R_{KI} is capped at 100 tokens. To
 1112 inject external clinical knowledge, we construct an
 1113 external knowledge base aligned with the predicted
 1114 disease label set L_k (refer to Appendix C). Dur-
 1115 ing generation, we retrieve the top- $k_t = 10$ most
 1116 relevant knowledge tokens via semantic similar-
 1117 ity.¹ All experiments were supported by an Intel(R)
 1118 Xeon(R) Silver 4215R CPU with 256 GB RAM,
 1119 and inference was set with $m = 5$.

1121 E Ablation Analysis on IU Dataset

1122 We further validate each component on the IU
 1123 X-Ray dataset as detailed in Table 5. The base
 1124 encoder-decoder achieves a BL-1 score of 0.435.
 1125 Adding standard visual-textual alignment in model
 1126 (a) improves average performance by 5.4%, while
 1127 incorporating the Prior-Guided Attention Module
 1128 in model (b) yields a performance gain of 8.2%,
 1129 highlighting the benefit of multi-view context. In-
 1130 troducing disease-aware supervision further im-
 1131 proves performance. Replacing standard align-
 1132 ment with Disease-aware Visual-Textual Contrast
 1133 in model (d) increases BL-1 to 0.498, surpass-
 1134 ing the prior-aware model (c) and demon-
 1135 strating stronger grounding from disease labels. Com-
 1136 bining PRAM with Di-VTC in model (e) increases the
 1137 score to 0.531. Injecting external clinical knowl-
 1138 edge into the model (g) further refines performance
 1139 to 0.553, confirming the value of domain-specific
 1140 context. The full framework in model (h), which
 1141 applies LLM-based QA restructuring, achieves the
 1142 best results across all NLG metrics with a 28.1%
 1143 average improvement over the base model. These
 1144 results are consistent with our MIMIC-CXR ex-
 1145 periments and confirm the robustness of CliQ-RRG.

1146 F Impact of LLMs on QA Restructuring

1147 We evaluate the impact of different LLMs on re-
 1148 structuring the intermediate report into QA for-
 1149 mat. Fig. 6 reports results on MIMIC-CXR and IU
 1150 X-Ray using BLEU-4, CE (F1), and BERTScore.
 1151 We compare closed-source models (GPT-3.5-turbo
 1152 (Achiam et al., 2023), GPT-5 (Achiam et al., 2023),
 1153 Gemini-3 Pro (Team et al., 2023)) and an open-
 1154 source model (Llama-3-8B-Instruct (Grattafiori
 1155 et al., 2024)) under zero-shot, few-shot, and
 1156 QLoRA fine-tuned settings. Few-shot prompting
 1157 consistently improves over zero-shot, while mod-

¹We tested top- $k_t \in [1, 15]$ and selected 10 for its optimal performance.

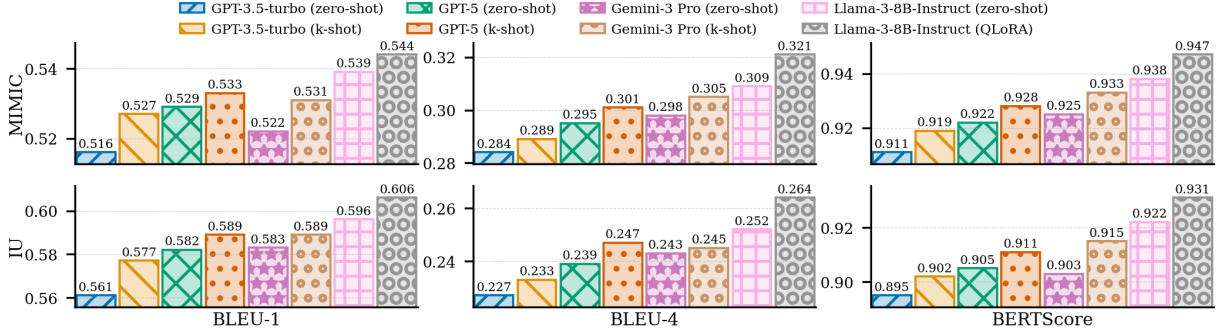


Figure 6: QA restructuring comparison across LLMs under zero-shot, few-shot, and fine-tuned settings on MIMIC-CXR and IU X-Ray using BLEU-4, CE (F1), and BERTScore.

Table 5: Ablation analysis on IU dataset showing incremental performance gains by integrating the PrAM, Di-VTC (across V_{ch} - T_{ch} and L_{ch}), \mathcal{K}_{ext} , and LLM-based components into the base configuration.

Model	STAGE 1			STAGE 2			NLG Metrics			
	PrAM	V_{ch}	T_{ch}	L_{ch}	\mathcal{K}_{ext}	LLM	BL-1	BL-4	MTR	RG-L
Base	✗	✗	✗	✗	✗	✗	0.435	0.144	0.174	0.387
(a)	✗	✓	✗	✗	✗	✗	0.452	0.168	0.184	0.398
(b)	✓	✗	✗	✗	✗	✗	0.468	0.165	0.196	0.404
(c)	✓	✓	✗	✗	✗	✗	0.489	0.194	0.205	0.418
(d)	✗	✓	✓	✗	✗	✗	0.498	0.188	0.201	0.411
(e)	✓	✓	✓	✓	✗	✗	0.531	0.207	0.213	0.425
(f)	✗	✓	✓	✓	✓	✗	0.544	0.211	0.217	0.429
(g)	✓	✓	✓	✓	✓	✓	0.553	0.216	0.221	0.434
(h)	✓	✓	✓	✓	✓	✓	0.561	0.227	0.230	0.442

PrAM: Prior-Guided Attention Module; V_{ch} : Visual Channel; T_{ch} : Textual Channel; L_{ch} : Predicted diagnostic label; \mathcal{K}_{ext} : External clinical knowledge. LLM: Large Language Model; ∇_N : Average improvement across all NLG metrics over the base configuration.

els such as GPT-5 and Gemini-3 Pro further improve restructuring quality. Fine-tuned Llama-3-8B-Instruct achieves the best overall performance, showing that lightweight task-specific adaptation is more effective than prompt design alone.

Since all LLMs operate on the same knowledge-injected intermediate report, diagnostic content remains unchanged; performance differences mainly reflect linguistic restructuring ability, indicating robustness to LLM choice.

G Computational Efficiency

We analyze the computational efficiency of CliQ-RRG on a single NVIDIA Tesla T4 GPU, as summarized in Table 6. The framework consists of a two-stage architecture with $\sim 170M$ trainable parameters, including STAGE 1 multimodal alignment and STAGE 2 report decoding. The average inference time of the pipeline is 150 ms per study, excluding the final QA restructuring step. Knowledge token retrieval introduces negligible overhead due to the fixed vocabulary and simple similarity search. The external LLM is invoked only once

per study for QA formatting via the GPT-3.5-turbo API and is not included in the local inference cost. This final restructuring step introduces a variable latency of 1.2 to 2.5 s and runs independently of the local inference hardware.

Table 6: Computational efficiency of CliQ-RRG

Method	Parameters	Inference Time
CliQ-RRG (Knowledge-Injected)	$\sim 170M$	150–250 ms / study*
CliQ-RRG (QA Pair)		1.35–2.75 s / study*

* : For Single-scan and prior scan.

H Practical Implication

CliQ-RRG offers several practical benefits for real-world clinical deployment and research use. First, the QA-style report formulation converts free-text narratives into a structured format that is easier to read, review, and query, which supports faster clinical decision making. Second, the disease-aware design ties each reported finding to explicit diagnostic evidence, thereby improving report consistency and enabling clinicians to verify conclusions with greater confidence. Third, the use of prior examinations supports longitudinal assessment and clearer tracking of disease changes across visits. Fourth, the integration of clinical knowledge enriches reports with relevant medical context, improving coverage of main findings without increasing text density. Finally, CliQ-RRG streamlines the radiology workflow by generating structured and reliable reports that clinicians can directly utilize.

I Future Work

Future work will focus on extending the framework along several methodological and practical dimensions. First, extending the framework toward Open-Set VQA generation is a promising direction

1209 for future work. Second, we will extend the frame-
1210 work to additional imaging modalities, including
1211 3D data such as CT and MRI, to assess its applica-
1212 bility to volumetric and anatomically complex sce-
1213 narios. Third, we plan to explore vision–language
1214 models that directly perform multimodal question
1215 answering in an interactive manner. Fourth, fu-
1216 ture evaluations will include multi-center and cross-
1217 institutional datasets to examine robustness across
1218 diverse clinical environments. Fifth, we aim to in-
1219 vestigate semi-supervised and weakly supervised
1220 learning strategies to reduce dependence on fully
1221 annotated data. Sixth, incorporating structured
1222 medical knowledge graphs will allow the model
1223 to capture disease relationships while preserving
1224 semantic knowledge retrieval.

1225 J Reproducibility

1226 To support reproducibility, we release our
1227 code at: [https://anonymous.4open.science/](https://anonymous.4open.science/r/CliQ-RRG)
1228 r/CliQ-RRG